Channel flow, tectonic overpressure, and exhumation of high-pressure rocks in the Greater Himalayas

Fernando O. Marques[1*], Nibir Mandal[2], Subhajit Ghosh[3], Giorgio Ranalli[4], Santanu Bose[3]

[1]Universidade de Lisboa, Lisboa, Portugal

[2]Jadavpur University, Kolkata, India

[3]University of Calcutta, Kolkata, India

[4]Carleton University, Ottawa, Canada

Abstract

The Himalayas are the archetype of continental collision, where a number of long-standing fundamental problems persist in the Greater Himalayan Sequence (GHS): (1) contemporaneous reverse and normal faulting; (2) inversion of metamorphic grade; (3) origin of high- (HP) and ultra-high (UHP) pressure rocks; (4) mode of ductile extrusion and exhumation of HP and UHP rocks close to the GHS hanging wall; (5) flow kinematics in the subduction channel; and (6) tectonic overpressure, here defined as $TOP = P/P_L$ where P is total (dynamic) pressure and P_L is lithostatic pressure. In this study we couple Himalayan geodynamics to numerical simulations to show how one single model, upward-tapering channel (UTC) flow, can be used to find a unified explanation for the evidence. The UTC simulates a flat-ramp geometry of the main underthrust faults, as proposed for many sections across the Himalayan continental subduction. Based on the current knowledge of the Himalayan subduction channel geometry and geological/geophysical data, the simulations predict that a UTC can be responsible for high *TOP* (> 2). *TOP* increases exponentially with decrease in UTC's mouth width, and with increase in underthrusting velocity and channel viscosity. The highest overpressure occurs at depths < -60

km, which, combined with the flow configuration in the UTC, forces HP and UHP rocks to exhume along the channel's hanging wall, as in the Himalayas. By matching the computed velocities and pressures with geological data, we constrain the GHS's viscosity to be $\leq 10^{21}$ Pa s, and the effective convergence (transpression) to a value $\leq 10\%$. Variations in channel dip over time (> or < 15º) may promote or inhibit exhumation, respectively. Viscous deformable walls do not affect overpressure significantly for a viscosity contrast (viscosity walls/viscosity channel) in the order of 1000 or 100. *TOP* in a UTC, however, is only possible if the condition at the bottom boundary is no outlet pressure; otherwise it behaves as a leaking boundary that cannot retain dynamic pressure. However, the cold, thick and strong lithospheres forming the Indian and Eurasian plates are a good argument against a leaking bottom boundary in a flat-ramp geometry, and therefore it is possible for overpressure to reach high values in the GHS.

Keywords: Himalayan geodynamics; channel flow; Greater Himalayas; numerical modelling; tectonic overpressure; exhumation HP and UHP rocks

*Corresponding author. E-mail address: fomarques@fc.ul.pt

1. Introduction

Continental collision has brought together two continents, India and Eurasia, which were previously separated by thousands of kilometres of oceanic lithosphere that has been consumed by subduction. Understanding the mechanics of the collisional interface, known as the Greater Himalayas Sequence (GHS), has continuously stimulated geoscientists to search for new concepts/models. Most critically, high- (HP) and ultrahigh- (UHP) pressure rocks crop out along the Himalayan GHS, thus raising long-standing and lively debated questions regarding formation and exhumation of HP and UHP rocks, and the difference between lithostatic and dynamic

pressures (overpressure) in dynamic systems. The GHS appears therefore as a unique natural prototype that can be modelled numerically in the search for answers to those critical questions.

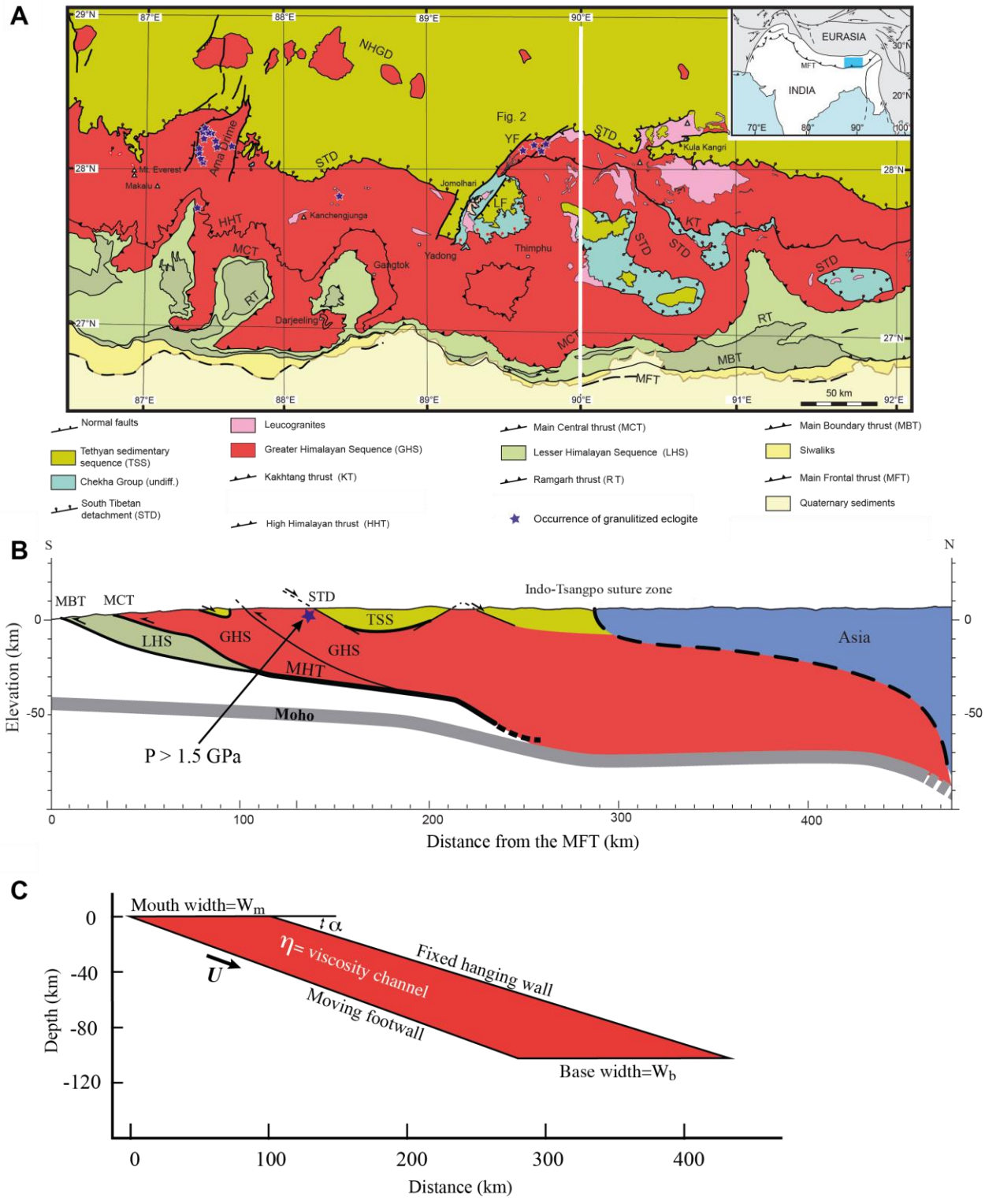

Figure 1. Geological setting of the eastern Himalayas, highlighting the architecture of its major tectonic elements. A – Simplified geological map of the eastern Himalayas (adapted from Grujic et al., 2011; Unsworth et al., 2005). White line along 90ºE marks the cross-section shown in B. B – Schematic section across the Himalayas (adapted from Grujic et al., 2011), in which the UTC stands out (GHS in red). The

GHS is bounded at the top by the South Tibet Detachment (STD) and at the bottom by the Main Central Thrust (MCT). MHT – Main Himalayan Thrust. C – Model setup of the UTC, with shape and dimensions similar to the natural prototype in B. The "foot wall" (moving wall) and the "hanging wall" (no slip wall) correspond to the MCT and the STD, respectively. Apart from the later folding of both MCT and STD, the similarity between nature and model setup is apparent.

1.1. Geological setting

Based on metamorphic grade and structural style, four units and the major faults separating them were distinguished by Gansser (1964), which are from bottom to top (Fig. 1): Sub-Himalayan Sequence (SHS – unmetamorphosed Tertiary rocks), Main Boundary Thrust (MBT), Lesser Himalayan Sequence (LHS – low-grade metamorphic rocks), Main Central Thrust (MCT), Greater Himalayan Sequence (GHS – high-grade metamorphic rocks), South Tibetan Detachment (STD), and Tethyan Sedimentary Sequence (TSS – unmetamorphosed to weakly metamorphosed rocks). All the main faults are N-dipping thrusts, except the STD that also dips to N but is a normal fault.

The GHS shows patchy occurrences of eclogites close to the STD (Grujic et al., 2011; Ganguly et al., 2000; O'Brien et al., 2001; Groppo et al., 2007; Corrie et al., 2010; Kellett et al., 2013; Sorcar et al., 2014; Zhang et al., 2015) (Fig. 1A). Recent petrologic studies provide estimates for spatial-temporal variations of pressure (P) and temperature (T) in the GHS. The peak metamorphic conditions are $T \sim 760$ °C and $P \geq 1.5$ GPa for eclogitization in the Bhutan Himalayas (Grujic et a., 2011). Peak conditions with $T = 670$ °C and $P \geq 1.5$ GPa were reported for the Nepal Himalayas (Corrie et al., 2010). On the other hand, an estimate of the metamorphic peak at $P = 2.7$–2.9 GPa and $T = 690$–750 ºC from coesite-bearing eclogites in the western Himalayas was provided by O'Brien et al. (2001). The eclogites have been in part overprinted by regionally more extensive granulite facies conditions of 800 °C at ~ 1 GPa (Grujic et al., 2011; Ganguly et al., 2000; Groppo et al., 2007; Zhang et al., 2015). *PT*-time paths suggest exhumation of these high-grade rocks under nearly isothermal decompression after peak metamorphic conditions (Ganguly et al., 2000; Groppo et al., 2007; Sorcar et al., 2014). Using cooling rates,

the exhumation history of the high-grade rocks was interpreted as a two-stage event by Ganguly et al. (2000), marked by exhumation at a rate of 15 mm/yr to a depth of 15 km, followed by slow exhumation at a rate of 2 mm/yr to a depth of at least 5 km, which occurred broadly in Miocene times (Grujic et al., 2011; Corrie et al., 2010; Kellett et al., 2013; Sorcar et al., 2014; Warren et al., 2011; Rubatto et al., 2013).

The exhumation mechanics of GHS rocks is one of the most debated issues in the Himalayas (and elsewhere where HP and UHP rocks outcrop), having led to a variety of tectonic models that postulate channel flow by topographic forcing (Wobus et al., 2005; Beaumont et al., 2001) or transpression (Grujic et al., 1996). Grujic et al. (1996) first proposed the GHS in the Bhutan Himalayas as deep crustal ductile rocks extruded between the MCT and the STD. Numerical models have integrated geological, tectonic, geophysical, metamorphic and rheological data to provide possible explanations for the exhumation process. The models postulate a channel flow of low-viscosity rocks in the middle to lower crust, driven by topographic pressure gradient, to account for the extrusion dynamics of high-grade metamorphic rocks in the GHS (Wobus et al., 2005; Beaumont et al., 2001). The channel flow model can also explain the coeval reverse and normal kinematics along the MCT and STD, respectively (Fig. 1B). However, as Grujic et al. (2011) pointed out, these models cannot "*predict the exhumation of lower orogenic (>50 km, i.e. >1.4 GPa) crustal material*" in their basic form. To overcome this limitation, an alternative exhumation mechanism was proposed by Grujic et al. (2011), with additional tectonic forcing (transpression) by the impingement of strong Indian crust into the already weak lower crustal granulitized eclogites below southern Tibet. However, previous models do not comprehensively address the mechanics of overpressure leading to the formation of eclogites (Schulte-Pelkum et al., 2005), and their focused exhumation close to the STD.

Given that the current models do not fully explain the observations in the GHS, in this study we couple eastern Himalayan geodynamics with numerical simulations to show how one

single model, upward-tapering channel (UTC) flow, as in the current eastern Himalayas (Fig. 1B), can be used to find a unified explanation for the following persisting problems: (1) contemporaneous reverse and normal faulting; (2) inversion of metamorphic grade; (3) origin of high- (HP) and ultrahigh- (UHP) pressure rocks; (4) mode of ductile extrusion and exhumation of HP and UHP rocks close to the GHS hanging wall (STD); (5) flow kinematics in the subduction channel; and (6) tectonic overpressure.

1.2. Premises

We model channel flow with a linear viscous fluid by the Navier-Stokes equation with body force (gravity), therefore pressure in the channel depends on viscosity and velocity configuration. Most critically, the velocity field depends on channel geometry and conditions applied at the boundaries (e.g. Marques et al., 2018). Ultimately, *TOP* can only exist if the channel walls are strong enough. Therefore, when investigating pressure in a viscous channel, one has to take into account four fundamental issues:

(1) *Viscosity* – the viscosity term in the Navier-Stokes equation depends on a number of parameters, all of which are incorporated in the Arrhenius term in a constitutive equation. Therefore, the modeller has two options when investigating the effects of viscosity on pressure: either use a full constitutive equation and test all the parameters in the Arrhenius term, or simply and directly vary the magnitude of the viscosity. We chose the second option in our numerical simulations, since our focus is the assessment of parameter variations on the development of overpressure and flow configuration.

(2) *Geometry of the channel* – given that flow configuration inside the channel plays a critical role in the pressure distribution, we tested three main shapes of the channel: parallel-sided (parallelepiped), and upward (similarly to Marques et al., 2018) or downward tapering channels.

(3) *Boundary conditions* – the conditions at the boundaries can either promote or inhibit *TOP*, because they control the flow pattern and the pressure retention inside the channel. Therefore, we tested different velocity configurations applied at the underthrusting (foot) wall (simple or simple+pure shears), and different conditions at the boundaries like slip, no-slip or outlet pressure.

(4) *How the walls of the pressure vessel react to internal pressure* – under particular applied boundary conditions, the Navier-Stokes equation produces *TOP* in an upward tapering channel that can reach values orders of magnitude greater than observed in nature; therefore we will discuss the theoretical values in view of the current knowledge on natural HP and UHP rocks. The discussion of channel flow is similar to discussing a pressure vessel with an overpressured fluid inside: one has to investigate the conditions to produce overpressure inside the vessel (the channel in the prototype), and simultaneously the strength of the vessel walls (the lithosphere in the prototype) to support the internal pressure without failure (by brittle or viscous yield). We will therefore discuss the strength of the channel walls in view of the current knowledge about the Indian (footwall) and Eurasian (hanging wall) lithospheres, especially in terms of thickness and strength.

This study builds on the conceptual work by Marques et al. (2018) on tectonic overpressure.

Given the above premises, we investigated the conditions under which overpressured rocks can form and be exhumed in a prototype like the Himalayas: geometry of the channel, conditions at the boundaries, applied velocities, and viscosity. Based on the numerical simulations and the current knowledge of the Himalayas, we discuss the theoretical values of overpressure, the obtained exhumation velocities, the most likely viscosity of the subducted rocks, and finally the effects of the strength of the channel walls on overpressure.

2. Numerical modelling

We modelled the subduction channel, as illustrated in Fig. 1C, with an incompressible linearly viscous fluid, which has been accepted as a simple but effective approximation to the behaviour of rocks undergoing ductile flow. The setup simulates a flat-ramp geometry of the main underthrust faults, as shown in many cross-sections of the Himalayas, in particular the one shown in Fig. 1B. For steady-state flow of a viscous incompressible Newtonian fluid at very low Reynolds number, the dynamic Navier-Stokes equations reduce to the Stokes approximation, which is the basis of the COMSOL code for computational fluid dynamics used here.

2.1. Boundary conditions and model setup

The boundary conditions were as follows (see Fig. 1C, and Methods in Appendix for further details): (1) slab-parallel velocity ($\boldsymbol{U}$) applied on the underthrusting (foot)wall (2 to 20 cm/yr) (Feldl and Bilham, 2006; DeMets et al., 2010), and fixed hanging wall; (2) viscosity (η) between 10^{19} and 10^{22} Pa s (Beaumont et al., 2001; England and Houseman, 1989; Copley et al., 2011); (3) channel dip α (15-30º); (4) channel mouth's width W_m = 25 to 100 km, and width at the channel's base W_b = 150 or 200 km, from which we define $W_m^* = W_m/W_b$; (5) constant density of the material in the channel (2800 kg/m^3). Given the viscosity contrast between foot/hanging walls of the GHS and channel material, the channel walls were assumed undeformable in the first simulations, except when testing the effects of non-rigid walls on overpressure.

The metamorphic processes occur in response to the total isotropic stress, called *dynamic pressure*, which is a sum of the tectonic (Stokes) and lithostatic pressures (ρgz, where ρ is density, g is gravitational acceleration, and z is depth). We evaluate the dynamic pressure to explain the occurrence of high-pressure rocks in the GHS, and we define an overpressure factor (*TOP)* as the non-dimensional ratio between dynamic and lithostatic pressures (Figs. A1 and

185 A2). For a better understanding of overpressure in a UTC, we carried out a parametric study of
186 *TOP* as a function of η, W_m, α, $\boldsymbol{U}$, and effective convergence velocity (transpression) (see
187 Methods in Appendix for details). The prime focus of our investigation concerned the
188 simulations with $\boldsymbol{U}$ = 5 cm/yr, $\alpha = 20^o$, W_m = 100 km and W_b = 150 km, which represent the most
189 common and conservative values. We then use the numerical results to constrain the viscosity,
190 pressure and velocity in the channel, consistent with current geological data and estimates.
191
192 **3. Model results**
193 *3.1. Flow patterns*
194 The model UTC shows two main layers, one flowing downward due to applied
195 underthrusting motion in the footwall, and another flowing upward and so inducing relative
196 normal faulting on the hanging wall (Fig. 2). Two distinct flow cells exist, one as an open circuit
197 in the shallow channel (< 30 km depth), and another as a closed circuit in the deeper channel.
198 The line of flow reversal (dashed white line in Fig. 2B) acts as an internal large-scale shear zone
199 with curved geometry and thrust motion. The upward flowing layer shows, at shallow depth, a
200 maximum velocity $\approx 0.5 \times 10^{-9}$ m/s, i.e. ~16 mm/year. The line of flow convergence separates
201 crustal materials of contrasting pressures, one towards the footwall with $P < 1.5$ GPa, the other
202 towards the hanging wall with $P > 1.5$ GPa (red curve in left hand panel in Fig. 2D), which is the
203 pressure at which eclogite formation is possible at -30 km. Overall, the flow pattern shows that
204 significantly overpressured rocks (*TOP* > 2.) can be exhumed rapidly through a narrow region
205 close to the hanging wall of the channel, which corresponds to the STD in the Himalaya and
206 where HP and UHP rocks have been found.
207
208 *3.2. Dynamic pressure and overpressure*
209 Model results are presented as colour maps (Fig. 2) and graphs (Fig. 3), the latter

showing the effects of several parameters on overpressure in the subduction channel.

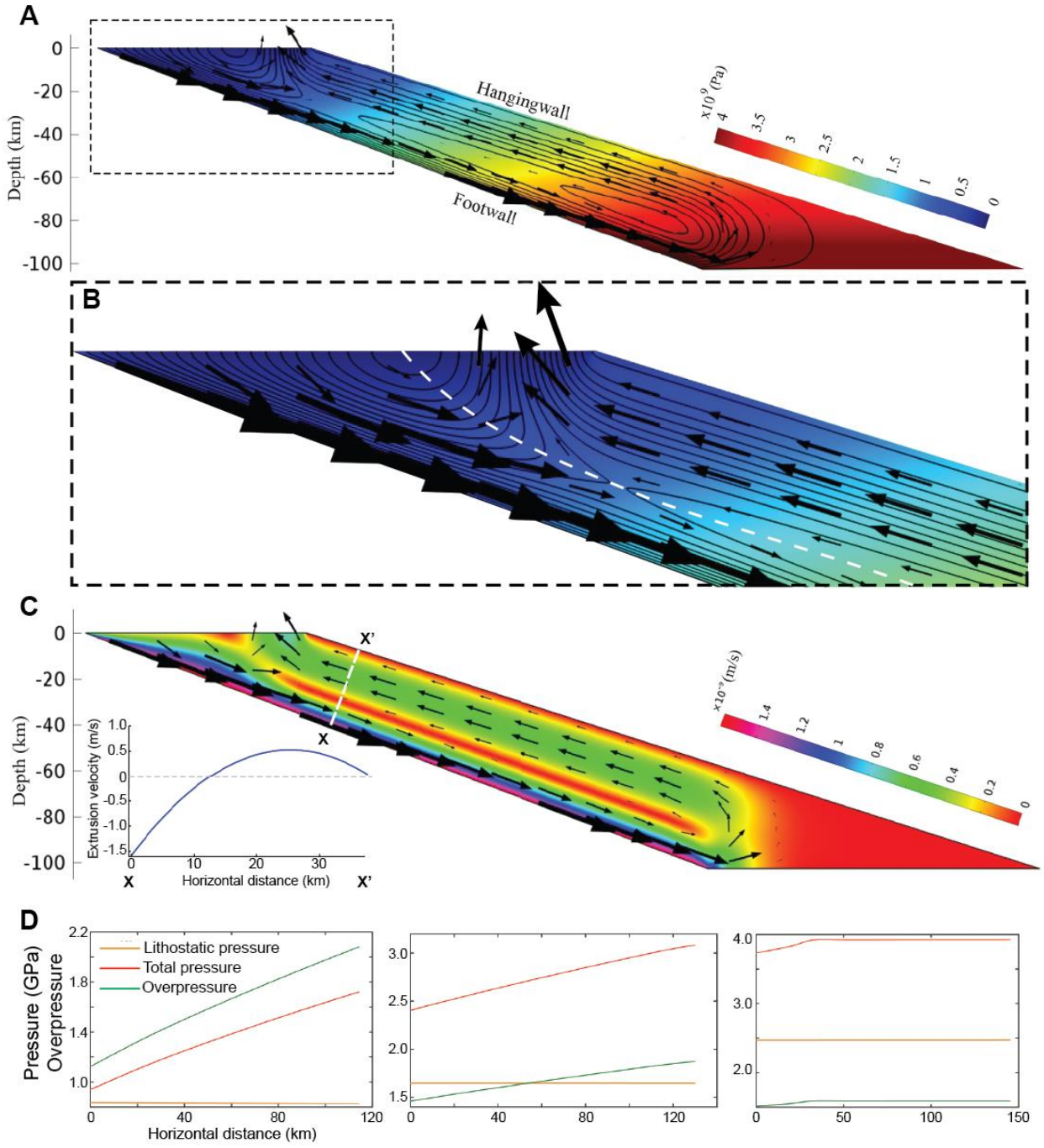

*Figure 2. Pressure and velocity maps and graphs for a UTC with α=20º, W_m=100 km, W_b=150 km, **U** = 4 cm/yr, and $\eta = 10^{21}$ Pa s. A – Velocity vectors and streamlines superimposed on pressure map (background colour and colour bar), where two distinct flow circuits can be recognized, one above and the other below -30 km. Also note asymmetry of flow relative to channel, with upward return flow concentrated nearest the hanging wall. B – Zoom of the topmost domain of the channel (marked by dashed rectangle in A). Note the convergence toward the surface between a shallow flow (mostly on the footwall side and carrying lower pressure and overpressure as seen in D) and a deep flow (mostly on the hanging wall side and carrying higher pressure and overpressure as seen in D). White dashed line separates downward and upward flows. C – Velocity vectors superimposed on velocity coloured map (colour bar for scale). Note*

the red stripe of lower velocity closer to the footwall, which corresponds to the line of flow reversal in the model. Inset in C showing a velocity profile across the channel (marked by white dashed line and X-X'). D – graphs showing P, PL and TOP = P/PL at -30, -60 and -90 km. Note that the highest overpressure occurs at the shallowest depth, and increases toward the hanging wall (except at -90 km).

Varying W_m with other parameters constant and $\eta = 10^{21}$ Pa s shows that the UTC develops overpressure in the entire range of $W_m/W_b = W_m^* = 25/150$ to 100/150 km (Fig. 3A). *TOP* is inversely proportional to W_m^*, and can be as high as 10 for $W_m^* = 0.17$ at depths between 20 and 60 km, with the highest *TOP* at 20 km depth.

TOP is sensitive to α in a UTC under a given set of values for W_m, η and $\boldsymbol{U}$ (Fig. 3B). The results plotted in Fig. 3B show *TOP* > 1 for $15^o < \alpha \leq 30^o$. *TOP* is maximal at α = 20-25°, reaching 1.7 at depths between 40 and 60 km.

The plot in Fig. 3C shows increase in *TOP* with increase in $\boldsymbol{U}$, from *TOP* ≈ 1.5 at $\boldsymbol{U}$ = 2-5 cm/yr (current Indian velocity), to *TOP* ≈ 11 when $\boldsymbol{U}$ = 20 cm/yr (Indian velocity at 60-70 Ma).

The simulations show a near-exponential variation of *TOP* with η (Fig. 3D), which we use to constrain the viscosity in the Himalayan collision zone.

Above we presented numerical simulations for $\eta = 10^{21}$ Pa s, typically applicable to the Himalayan tectonic setting. However, we ran additional simulations with different viscosities, and a set of results is presented for a viscosity of 10^{22} Pa s (Fig. 4). $\eta = 10^{22}$ Pa s induces much higher overpressure, especially when the mouth width decreases, and when the underthrusting velocity increases to velocities that have been estimated to exist at 60-70 Ma.

Taken together, the results shown in Figs. 3 and 4 place constraints on the factors affecting overpressure. Extremely high values of *TOP* are obtained for $\eta > 10^{21}$ Pa s, $U > 5$ cm/yr, and $W_m^* < 0.50$.

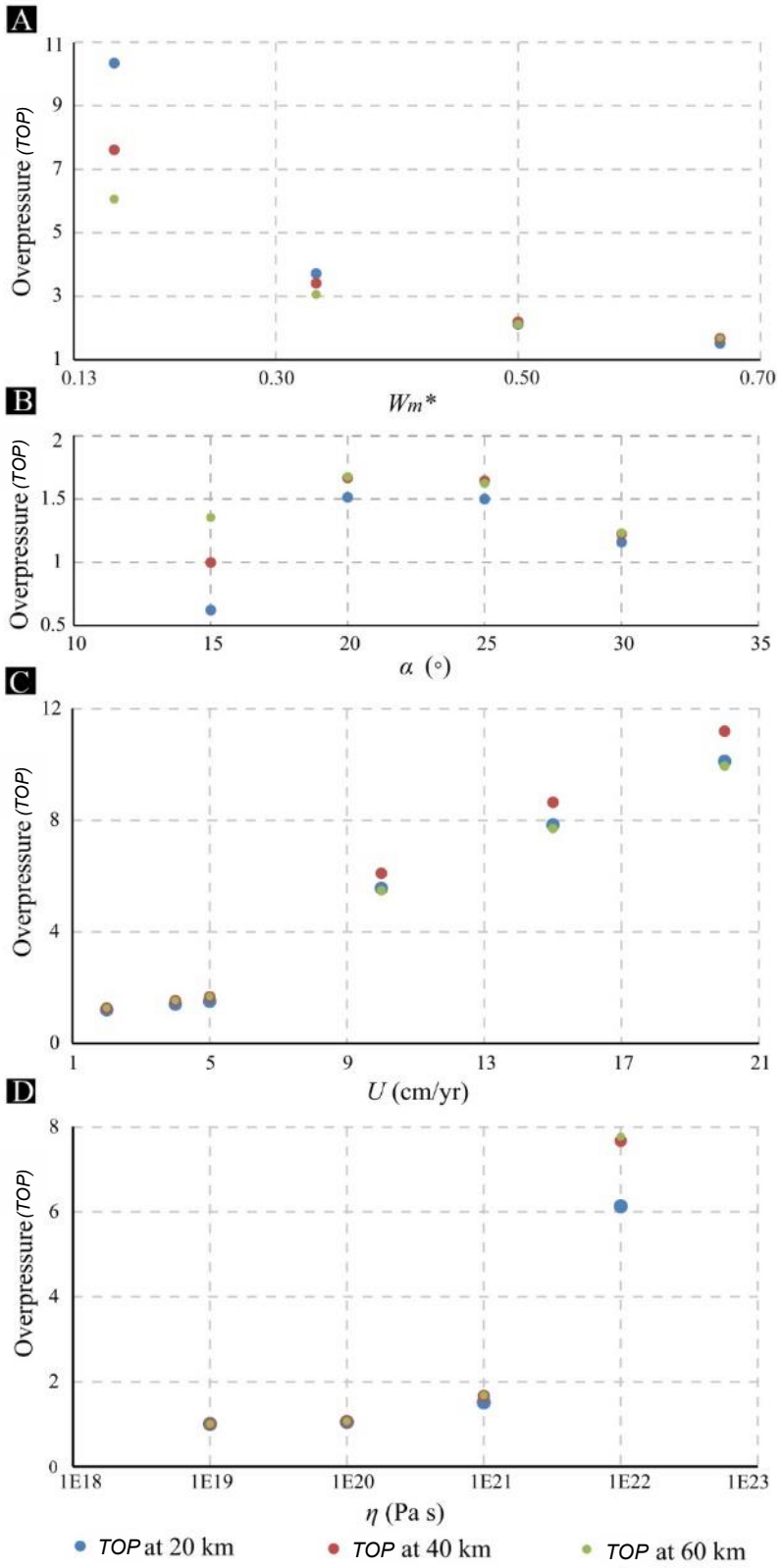

Figure 3. Graphs showing the dependence of overpressure factor (TOP) on normalized width of channel mouth W_m (A), channel dip α (B), underthrusting velocity **U** (C), and viscosity in the channel η (D). For each tested variable, other values are kept constant: W_m* = 100/150 = 0.67 (except in A), α = 20º (except in B), U = 5 cm/a (except in C), $\eta = 10^{21}$ Pa s (except in D).*

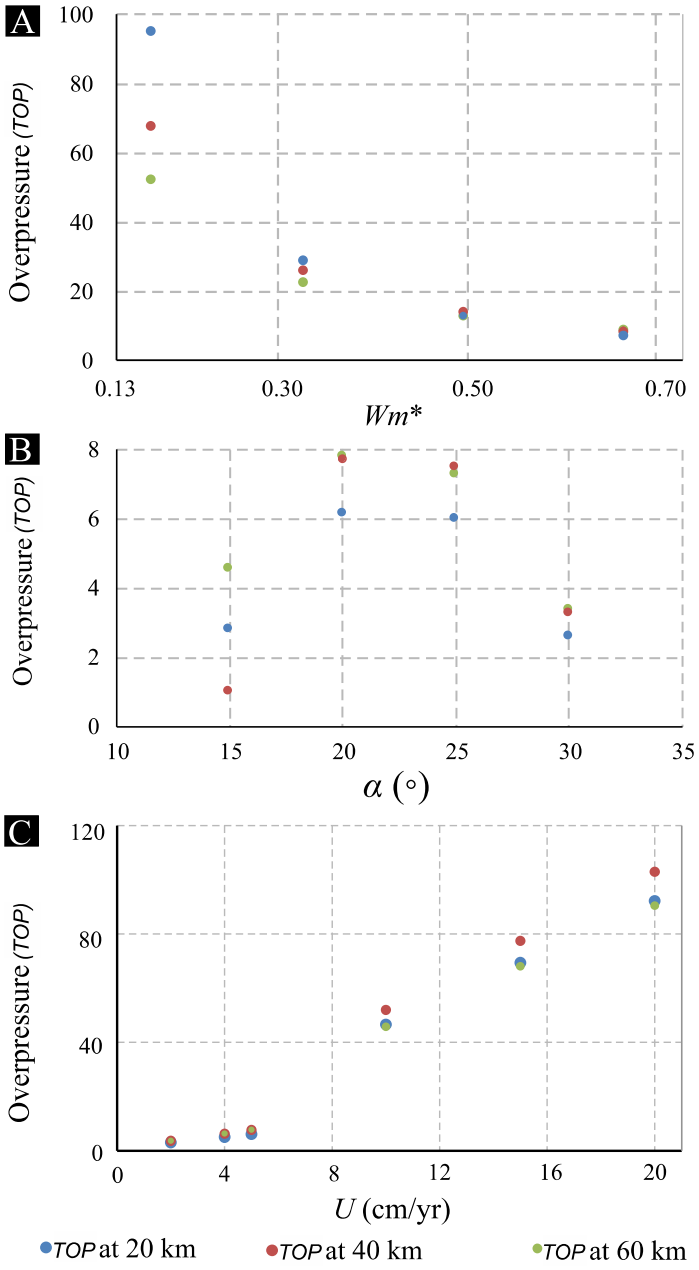

Figure 4. Graphs showing overpressure factor TOP as a function of normalized channel's mouth width W_m (A), channel dip α (B), and convergence velocity **U** (C), for a viscosity $\eta = 10^{22}$ Pa s. For each tested variable, other values are kept constant: W_m* = 100/150 = 0.67 (except in A), $\alpha = 20^o$ (except in B), U = 5 cm/a (except in C). Comparison with Fig. 3 shows that $\eta = 10^{22}$ Pa s induces much higher overpressure, especially at smaller W_m* and higher **U**.*

Varying channel dip (α) involves significant changes in the flow pattern, as shown in Fig. 5. For $\alpha = 15^o$, the channel is dominated by downward flow, setting in a large-scale vortex in the deeper level, and does not show conspicuous zones of ductile extrusion, which only occurs when $\alpha > 15^o$.

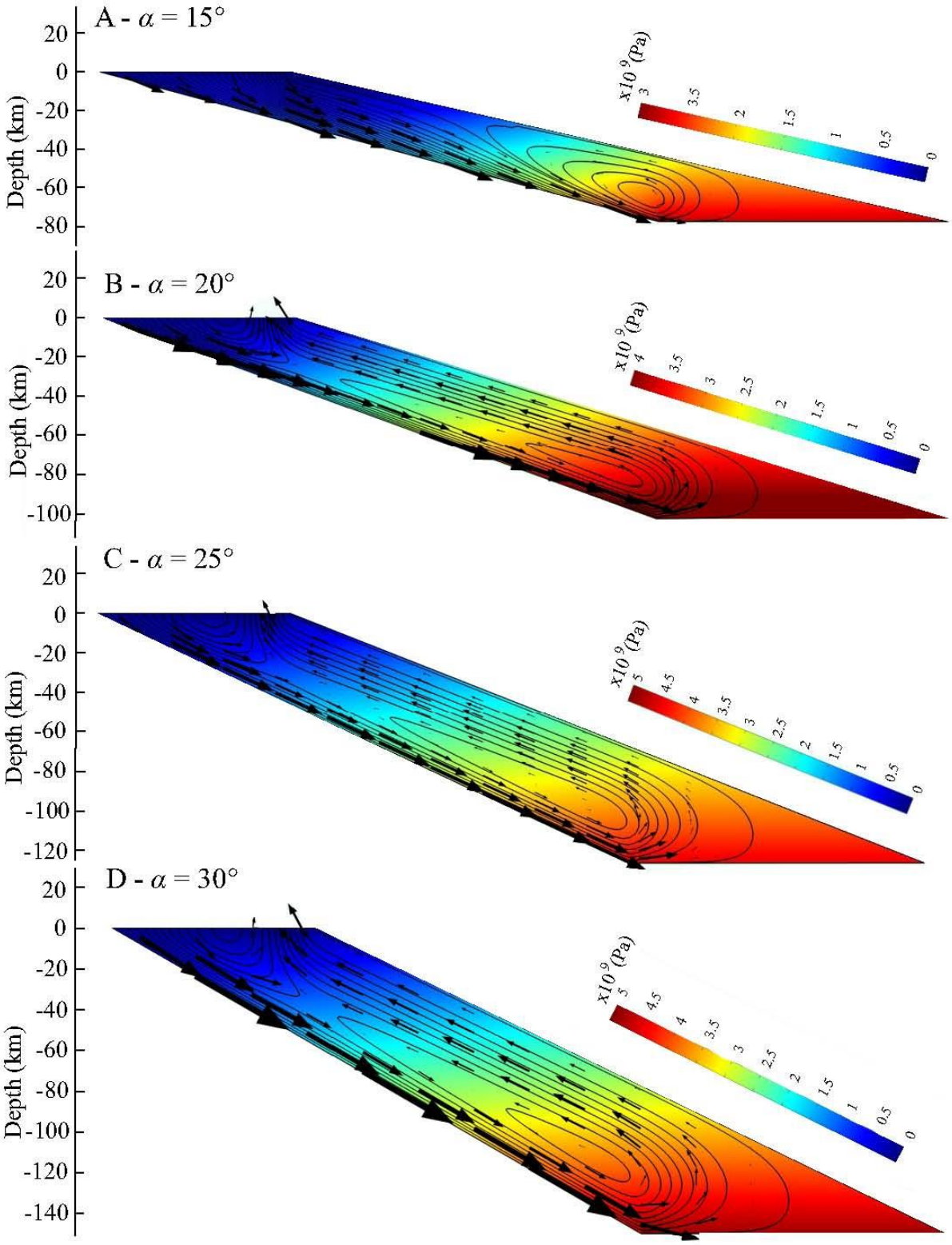

Figure 5. Simulations showing the effects of channel dip (α) on flow pattern.

Besides the results obtained for a channel base width of 150 km, and variable mouth

width, we also evaluated the effects of the channel base width on flow patterns and pressure distribution, by running a set of numerical simulations with a base width of 200 km. The channel flow shows similar patterns in the two cases, and small variations in pressure.

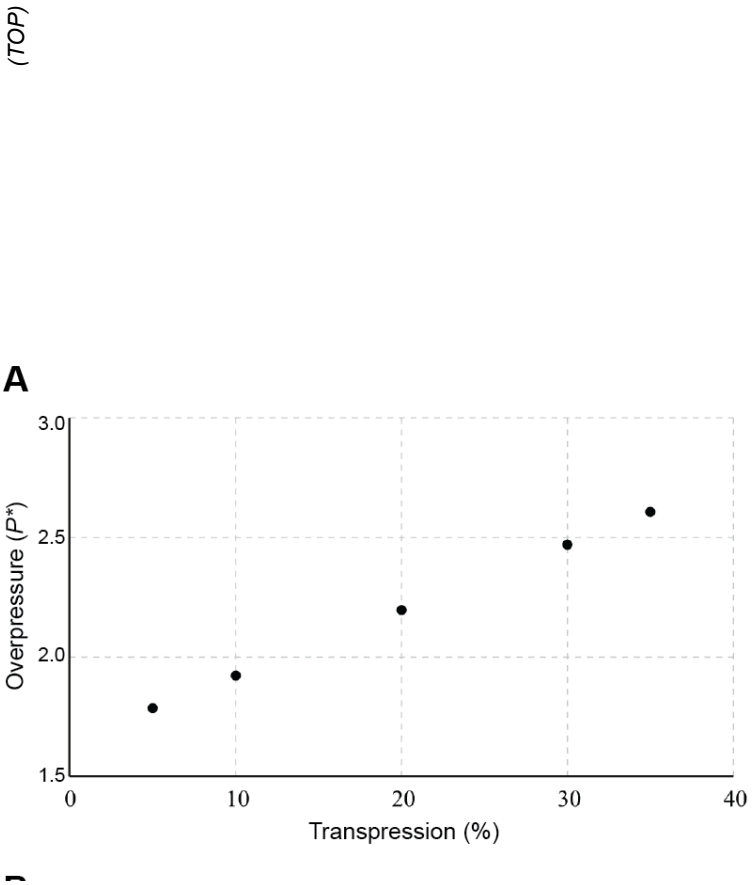

Figure 6. Graphs showing the linear dependence of overpressure (TOP)(A) and extrusion velocity (B) on transpression.

3.3. Effects of transpression on overpressure and flow

We ran a set of simulations to investigate how much a transpressional movement across the viscous channel might influence the magnitude of tectonic overpressure and, especially, velocity at the channels mouth (extrusion velocity). Transpression in the numerical models was introduced by setting the magnitude of horizontal velocity in excess of that corresponding to the

underthrusting movement. Fig. 6 shows a plot of *TOP* as a function of transpression, represented as the ratio between horizontal velocity and non-transpressional horizontal component (ca. 1.49E-9 m/s). The numerical results indicate that: (1) transpression has appreciable effects on overpressure, especially if transpression is large (> 20%); (2) transpression has great effects on extrusion velocity, as shown in Figs. 6 and 7.

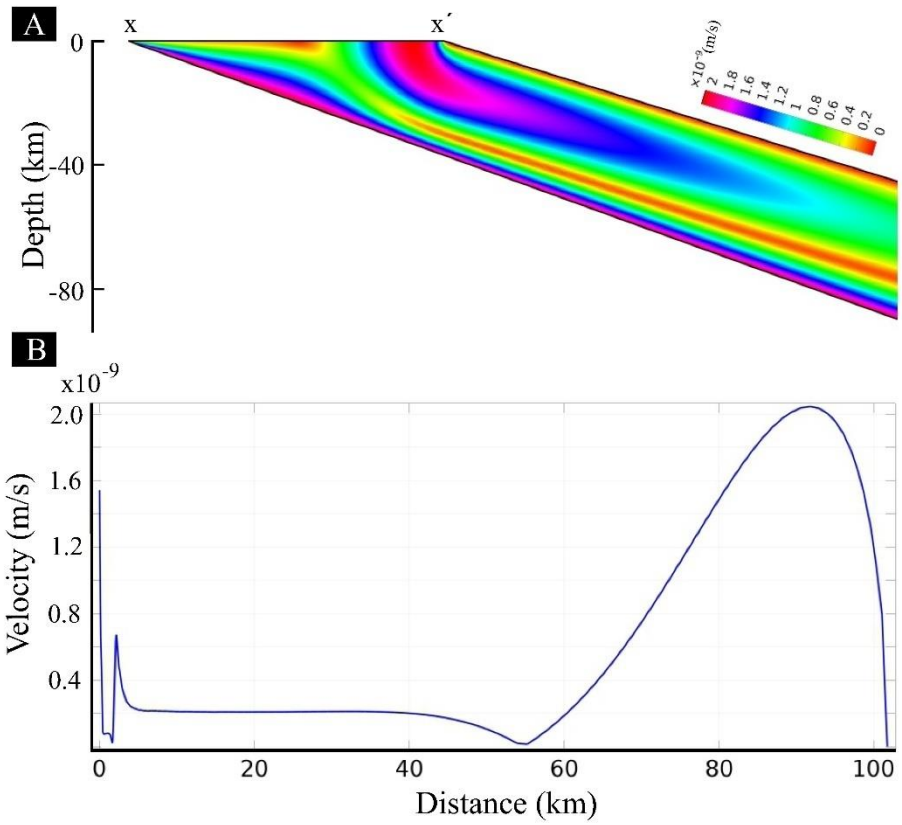

Figure 7. A – Velocity map of a channel under transpression. X-X' marks the line along which extrusion velocity was measured and plotted in B.

3.4. Viscous deformable walls

We used a similar modelling approach to evaluate the magnitude of overpressure in subduction channels confined by deformable walls, a model condition that closely replicates the actual mechanical setting in the Himalayas. This model allows for both channel walls to deform viscously, thus raising the question of how much overpressure they can retain inside the channel. We developed the deformable wall models with a channel geometry similar to that in rigid wall

models, as shown in Figure 8A. The footwall and the hanging wall of the channel were rheologically modelled as a viscous material, which provides a good approximation for simulation of long term (millions of years) rheology of the lithosphere. Several earlier workers have used viscous rheology to model continental scale deformation during India-Tibet collision. The assumed viscosity values of the cold Indian craton range from 10^{23} to 10^{25} Pa s (e.g. Jiménez-Munt and Platt, 2006; Yang and Liu, 2013), whereas that of Himalayan subducted material ranges between 10^{20} and 10^{21} Pa s (e.g. Liu and Yang, 2003; Copley and Mckenzie, 2007). The viscosity ratio (viscosity walls/viscosity channel) is therefore in the order of 10^2 to 10^5. In our modelling we chose a conservative value of the viscosity ratio equal to 10^3, where the walls and channel viscosities are 10^{23} and 10^{20} Pa s, respectively. We constrained the model boundaries with kinematic conditions as in the reference model with rigid walls. The lateral and the top boundaries of the footwall were subjected to a velocity of 4 cm/yr sub-parallel to the channel, whereas the lateral vertical boundaries of the hanging wall were fixed with zero horizontal velocity components, leaving the vertical component unconstrained. Its top boundary was also left unconstrained, allowing the material to extrude upward freely. The wall-channel interfaces had a no-slip condition.

Model results show channel flow patterns quite similar to those observed in rigid wall models. The extrusion occurs along a region close to the hanging wall in the form of a Poiseuille flow (Fig. 8A). It is noteworthy that the footwall undergoes little or no deformation, although being deformable. The entire footwall underthrusts by translational motion parallel to the channel. We calculated both the dynamic and the static pressures along the channel axis, and plotted them as a function of depth (Fig. 8B). Similarly to rigid wall models, the dynamic pressure here exceeds the static pressure by nearly 1.5 GPa. For example, the static pressure at a depth of 60 km is about 1.5 GPa, whereas the corresponding dynamic pressure reaches 3 GPa. The pressure plots clearly suggest that subduction channels with deformable walls can also give

rise to large tectonic overpressures. For a viscosity ratio of 10^3, the deformable wall models are found to be mechanically identical to rigid wall models.

We also used a lower viscosity contrast of 10^2, and found that even at this relatively low contrast there is significant overpressure in the subduction channel.

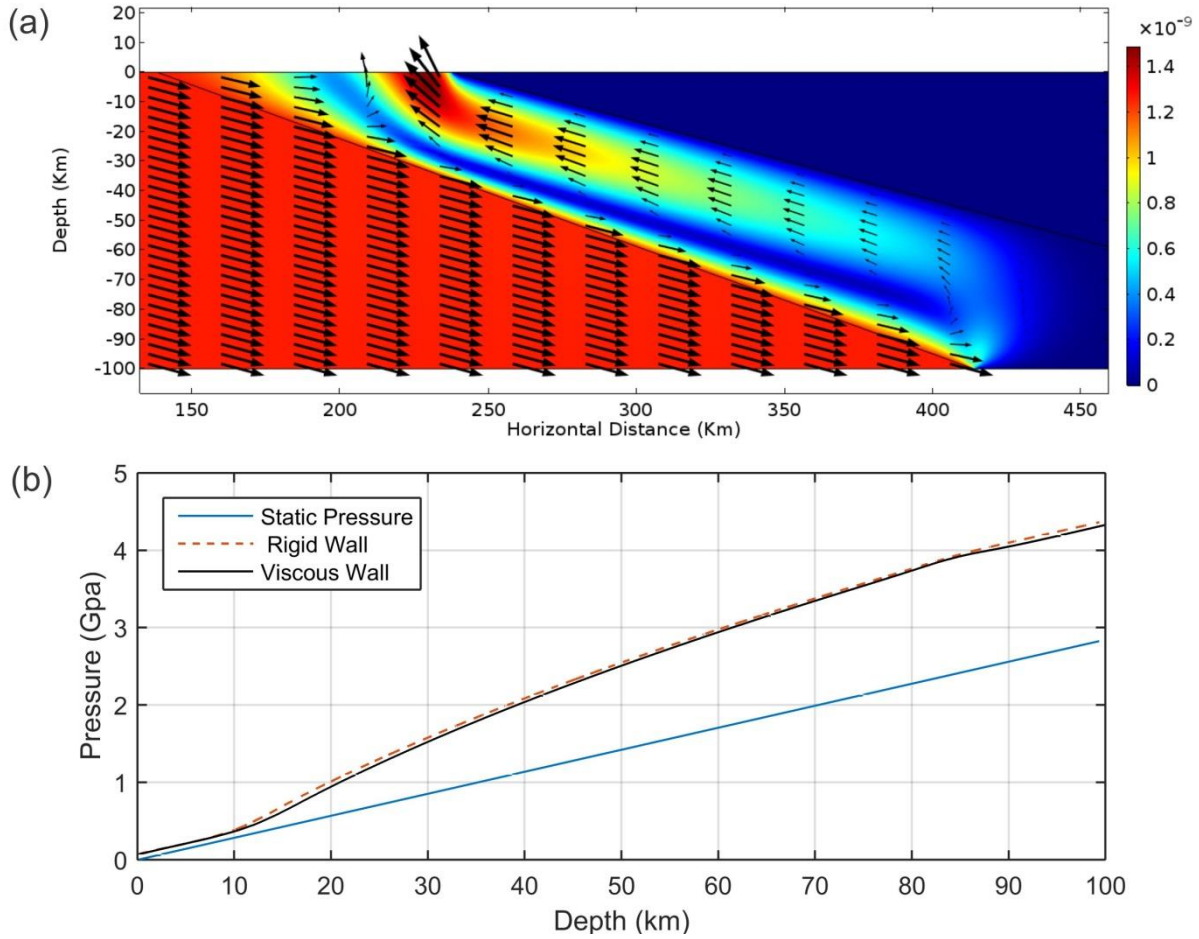

Figure 8. A – Crustal flow patterns in viscous subduction channel and its deformable walls with a viscosity ratio of 10^3 (details of model boundary conditions in the text). B – Calculated plots of pressure as a function of depth along the channel axis. Note that the dynamic pressure obtained from deformable wall models with viscosity contrast 1000 closely follows that for channels with rigid walls.

3.5. Condition at the bottom boundary

This is a critical boundary condition because it is directly related to the retention of overpressure. When we assign an outlet pressure (calculated lithostatic pressure at the depth of the bottom wall) to the bottom wall, *TOP* does not develop in the whole channel.

4. Discussion

4.1. Comparison with previous work

The occurrence of TOP has received much attention in the geological literature (e.g. Rutland, 1965; Mancktelow, 1993, 1995, 2008 and references therein; Petrini and Podladchikov, 2000; Schmalholz and Podladchikov, 2013; Schmalholz et al., 2014b). TOP has been argued to exist in both hard (Mancktelow, 1993) and soft (Mancktelow, 1995) layers, and its occurrence has been predicted by force balance considerations independent of rheology (Schmalholz and Podladchikov, 2013; Schmalholz et al., 2014a, 2014b). We have previously explored (Marques et al., 2018) the occurrence of TOP in higher viscosity layers intercalated in lower viscosity layers (layer-parallel shortening of a rheologically stratified lithosphere), and in a lower viscosity layer between higher viscosity walls (subduction zone).

Previous work has investigated the occurrence of TOP at all scales: (1) local variations in pressure (e.g. Mancktelow, 1993; Tenczer et al., 2001; Taborda et al., 2004; Marques et al., 2005a, 2005b, 2005c, 2014; Schmid and Podladchikov, 2003, 2004; Ji and Wang, 2011; Schmalholz and Podladchikov, 2014; Tajčmanová et al., 2014, 2015; Angel et al., 2015), which in many cases is the natural consequence of the use of Stokes flow in the model, similarly to the numerical model used in the present study; (2) TOP in subduction zones (e.g. Li et al., 2010; Reuber et al., 2016). Given the great dependence of pressure on geometry, boundary and ambient conditions, and flow pattern, we cannot compare our Stokes flow models directly with the cited self-consistent geodynamic models, because in these the controlling parameters are combined with many other variables and parameters that act simultaneously and change with time. Therefore, we analysed, separately, the effects of the various parameters and boundary conditions on pressure in order to gain a better understanding of the effects of each of them.

TOP has been investigated as a function of the tectonic environment (e.g. Stüwe and Sandiford, 1994; Petrini and Podladchikov, 2000; Vrijmoed et al., 2009; Pleuger and

Podladchikov, 2014; Schmalholz et al., 2014a), and geometrical effects on TOP have also been addressed (e.g. Schmalholz and Podladchikov, 1999; Moulas et al., 2014), e.g. in downward tapering (e.g. Mancktelow, 1995, 2008 and references therein) and parallel-sided subduction channels, which have been argued to be the most appropriate configurations to model natural subduction zones. However, given the complexity and unsteady nature of subduction zones, the subduction channel can adopt all possible configurations, and the strictly parallel-sided configuration should be considered an exception rather than a rule, especially if we consider the 3-D, non-cylindrical, nature of subduction zones. Previous models have used two of the three main possible configurations of a subduction channel: parallel-sided and downward tapering, which have been shown to produce $TOP < 3$ (e.g. Li et al., 2010; Reuber et al., 2016). Here we investigated a different channel geometry, the upward tapering channel. In fact, the parallel-sided geometry corresponds to $W_m^* = 1$, which can thus be considered an end-member of the UTC. Therefore, we can compare numerical results of overpressure obtained for parallel-sided and UTC channels, by looking at the graph where we vary W_m^* (Fig. 3A). Our best explanation for this effect is that the narrower the mouth the higher the flow confinement, which results in increased velocity gradient in the channel flow, and therefore the dynamic pressure.

The formation and exhumation of high (HP) and ultra-high (UHP) pressure rocks is a persisting fundamental problem, especially regarding UHP rocks. The problem is even greater if one assumes that pressure estimated from paleopiezometry can be converted directly to depth, because then the UHP rocks must be exhumed from great depths. Several models have been proposed for the exhumation of HP and UHP rocks in several orogens (e.g. Hacker and Gerya, 2013; Warren, 2013; Burov et al., 2014a, 2014b): channel flow (e.g. England and Holland, 1979; Mancktelow, 1995; Grujic et al., 1996; Beaumont et al., 2001, 2009; Burov et al., 2001; Raimbourg et al., 2007; Gerya et al., 2008; Warren et al., 2008; Li and Gerya, 2009); eduction (e.g. Andersen et al., 1991; Kylander-Clark et al., 2012); buoyancy-driven crustal delamination

and stacking (e.g. Chemenda et al., 1995, 1996; Sizova et al., 2012); microplate rotation (e.g. Hacker et al., 2000; Webb et al., 2008); trans-mantle diapirism (e.g. Stöckhert and Gerya, 2005; Little et al., 2011; Gordon et al., 2012); and slab rollback (e.g. Brun and Faccenna, 2008; Faccenda et al., 2009; Vogt and Gerya, 2014; Malusà et al., 2015). No model has so far provided a complete and unique explanation. The UTC model presented here is a potentially unifying model, because it shows that it is possible to form rocks recording HP or UHP at depths < 60 km and to exhume them to the surface as a consequence of the flow configuration in the UTC.

Regarding the discrepancy between previous estimates of possible values of overpressure and ours, we call attention to two factors: (1) we use a subduction channel geometry, the UTC, not investigated previously; and (2) the values reported here are very large only for small W_m*, or $\boldsymbol{U}$ > 5 cm/a, or $\eta > 10^{21}$ Pa s. In other words, for relatively small tapering (W_m*), average plate tectonics velocities, and reasonable viscosities, the numerical results reported here for overpressure are not excessive, but nevertheless still very important as a factor for depth overestimation. The values used for the controlling parameters, W_m*, α and η are conservative; in fact, the model channel in Fig. 1C shows rather small tapering as compared with the cross-section in Fig. 1B, but, nevertheless, the model overpressure is still quite high, especially at low depth.

4.2. Meaning and applicability of the numerical results

The numerical simulations reported here clearly discriminate the conditions favourable or unfavourable to the development of high TOP. The conditions that favour high TOP shallow in the subduction channel are: upward tapering geometry, high viscosity (> 1E20, which also means relatively low temperature), strong channel walls, general shear (i.e. simple + pure shears), low subduction angle, no-slip condition at the bounding lateral walls, and no-outlet condition at the bottom wall. All these conditions do not need to act simultaneously to generate TOP. We

conclude that, if during the unsteady evolution of a subduction zone, the boundary conditions, geometrical configuration and ambient conditions meet the favourable model setting here reported, then high TOP can develop. Otherwise, only small TOP can be expected. In great contrast, the single action of low viscosity, or downward tapering geometry, or weak channel walls, or outlet pressure at the bottom wall can prevent the development of TOP, or even promote underpressure.

We analysed the consistency between the numerical results and geological/geophysical data to constrain the most probable viscosity and pressure, at the same time satisfying a reasonable velocity at the channel's mouth (i.e. exhumation rates) (Fig. 7). On the one hand, the viscosity of rocks comprising the lithosphere can vary between 10^{19} and 10^{23} Pa s. On the other hand, overpressure is sensitive to the viscosity within the UTC, increasing rapidly with increase in viscosity. Additionally, from the values shown in Figs. 3 and 4, the formation of HP rocks can occur at very shallow levels if $\eta = 10^{21}$ Pa s. However, despite the relatively wide range of possible viscosity values, $\eta > 10^{21}$ Pa s, combined with other favourable conditions, in a Himalayan UTC yields overpressures > 8. This means that, for $\eta = 10^{22}$ Pa s, a rock metamorphosed at 50 km depth would record a total pressure equivalent to the lithostatic pressure at a depth of 400 km, which is not acceptable on the basis of our current knowledge of subduction zone dynamics. Therefore, we propose that the viscosity in the subduction channel is probably in the range $10^{20} \leq \eta \leq 10^{21}$ Pa s.

The UTC simulations show that there is no need for gravitational collapse, buoyancy-controlled crustal exhumation, or orogen-perpendicular pressure gradient induced by a topographic gradient to explain simultaneous reverse and normal fault kinematics in the MCT and STD, or inverse metamorphic grade, or exhumation of HP rocks. We conclude that flow in a UTC, without the need for topography or density contrasts, can be responsible for these three simultaneous and seemingly paradoxical processes in the Himalayas.

An important question regarding TOP in nature still persists: why do we not see TOP in all subduction zones around the globe? On the one hand, our simulations indicate that roll-back subduction (transtension, in opposition to the favourable transpression) is unfavourable for the development of TOP. In contrast, collision-type subduction zones, like the Himalaya, with intervening old, cold and strong lithospheres are favourable for TOP. On the other hand, the recognition of TOP depends on methods and analytical technology, as shown by the most recent literature on petrology. There is growing evidence that TOP is recorded by minerals, as shown by Tajčmanová et al. (2014), Tajčmanová et al. (2015), Moulas et al. (2013, 2014) and Angel et al. (2015) (see also Menant et al., 2018). Constraints from host-inclusion elasticity show that TOP can greatly depart from lithostatic pressure; Angel et al. (2015) showed that deviations from lithostatic pressure in excess of 1 GPa can be readily produced in quartz inclusions within garnet in metamorphic rocks.

4.3. Comparison between model and nature

Inspired by the cross-section of the natural upward tapering channel shown in Fig. 1b, we investigated the effects of this geometry on TOP, and use it to find new explanations to the problems raised by the Himalayan geodynamics.

Given our incomplete knowledge of natural prototypes and the limitations of modelling very complex systems, we must distinguish between the theoretically and naturally possible values of overpressure. The study here reported for a UTC shows that relevant parameters like channel mouth width (W_m*), subduction dip (α), underthrusting velocity ($\boldsymbol{U}$) and viscosity (η) can produce very high overpressure; however, these theoretically possible values must be constrained by the current knowledge of the Himalayas, in particular exhumation velocities and spatial distribution, occurrence of HP and UHP rocks, and strength of the lithosphere bounding the subduction channel. Despite the natural constraints imposed by our knowledge of the current

Himalayas, one cannot ignore that, under specific boundary conditions, geometrical configurations and parameter sets that could have existed in the past (e.g. much higher subduction velocity), high values of overpressure are theoretically possible, which should guide us in the search of new evidence in the natural prototype.

Previous models can explain channel flow, but neither account for the exhumation of HP rocks (Rubatto et al., 2013), nor the exhumation velocities (Grujic et al., 2011) reported from the Himalayas. Our UTC model provides an alternative explanation for the pressure required for eclogite metamorphism (Hetényi et al., 2007; Zhang et al., 2014), and the process of rapid exhumation. For exhumation by extrusion to occur in the subduction channel, the flow pattern inside the channel must have a specific configuration, as in the UTC. In such a velocity configuration, underthrusting and exhumation on the channel's footwall add to produce enhanced overthrusting on the MCT, and above the MCT along the line of flow reversal. Conversely, exhumation (upward flow) on the hanging wall is greater than underthrusting and produces relative normal fault displacement on the STD, not because the block to the N of the STD (hanging wall) moves down, but because the rocks south of the STD (footwall) move up due to exhumation by extrusion.

Previous channel flow models can explain the exhumation mechanism, however they leave a number of problems unaddressed. Here we raise some of these issues, pointing to our UTC model as a unifying model to explain the GHS evolution:

(1) The classical channel flow model assumes that the entire GHS crustal mass thrusts up along the MCT, with concomitant normal motion on the STD (Poiseuille flow). However, recent studies have shown large-scale thrusts within the GHS (Grujic et al., 2011; Larson et al., 2015), suggesting a more complex kinematics of the extrusion process. The UTC model we propose here shows flow partitioning in the channel, leading to thrust-type shear localization within the model GHS.

(2) A typical channel flow model fails to explain the occurrence of HP rocks (> 1.5 GPa) close to the STD. Our UTC model yields an asymmetrical flow pattern in which HP or UHP materials extrude along a narrow zone located close to the STD.

(3) The assumption of lithostatic pressure raises two main problems: (i) a conceptual problem, because the subduction channel is dynamic, therefore the lithostatic and dynamic pressures are not identical; and (ii) a practical problem, because the exhumation velocities are calculated on the basis of depth estimated from ρgz (where z is depth), and not normalized by the overpressure. For instance, conversion of 2 GPa to depth using a static assumption (ρgz) yields a depth of ca. 70 km for a rock density of 2900 kg/m^3. However, the UTC flow develops an overpressure in the order of 2 at much smaller depths, and thereby yields lower exhumation rates, as compared to those calculated from petrologic modelling. Estimated metamorphic paths should reflect the shape of the isotherms in the subduction channel, which must have a relationship with velocity in order to carry cold rocks to depth, and preserve the HP and UHP mineral parageneses during exhumation.

(4) Model velocities in the channel and at the channel's mouth must be consistent with the values reported in the literature. Assuming lithostatic pressure, an exhumation rate of ~ 15 mm/yr to a depth of at least 15 km was estimated by Ganguly et al. (2000). An estimate of 22–44 mm/yr, and increasing linearly with depth, was provided by Grujic et al. (2011). According to the UTC dynamic model, the assumption of lithostatic pressure where *TOP* = 2 yields an overestimation of the exhumation velocity by a factor of 2. If this is the case, then the velocity estimates have to be divided by two (15/2 = 7.5 mm/yr, and 33/2 = 16.5 mm/yr). Our UTC model shows a high velocity layer with the materials flowing upward at a rate of 16 mm/yr at a depth of ca. 40 km, which is thus in agreement with the estimated average exhumation. The velocity map in Fig. 6 reveals variations of exhumation rates with depth, as predicted for the GHS in the Sikkim Himalaya by Ganguly et al. (2000), who showed that

the exhumation was rapid (15 mm/yr) to a depth of 15 km, and then decreased to ca. 2 mm/yr until a depth of 5 km. These values estimated for exhumation in the GHS constrain the theoretical values of overpressure numerically obtained by varying the amount of transpression. Transpression values > 10% imply velocities at the mouth (exhumation) much higher than estimated for the GHS, therefore we conclude that transpression must be very limited (< 10%).

(5) A critical issue regarding overpressure in a subduction channel is the strength of the channel walls to support high overpressure values. One of the most debatable boundary conditions in our modelling is the use of rigid walls. For this discussion, we can compare the subduction channel to a pressure vessel, in which the resistance of the vessel to internal pressure depends on two main parameters: the strength of the vessel (the lithosphere hosting the subduction zone), and the thickness of the pressure vessel walls (hoop stress). In nature, if the walls of the pressure vessel (subducting and overlying lithospheres) are old and cold, which is the case in the Himalayan collision, then their mechanical strength can be very high. If, additionally, the cold and strong lithosphere is thick, then the walls of the subduction channel can support high overpressure, as indicated by the numerical results with viscous deformable walls. Given that the Indian plate and the TSS above the STD are almost undeformed (attesting to the rigidity contrast between foot and hanging walls of the GHS) and thick, the channel walls were assumed undeformable in the reference simulations. In order to investigate the effects of viscous deformable walls on tectonic overpressure, we used viscosity contrasts (viscosity of channel walls/viscosity of subduction channel) down to 100, which are well within the accepted values of lithosphere viscosity (up to 10^{23} Pa s) and subducted material (down to 10^{19} Pa s). These simulations indicate that viscosity contrasts of 1000 or 100 do not change significantly the overpressure obtained with rigid walls. Another critical issue in overpressure build-up is the condition at the bottom boundary: if an outlet

pressure is assigned to the bottom wall, then this boundary behaves as a leaking boundary that cannot retain dynamic pressure. However, the cold, thick and strong lithospheres that comprise the Indian and Eurasian plates are a good argument against a leaking bottom boundary in a flat-ramp geometry such as the Himalayan collision zone. If, for some reason, the channel walls become weaker, in the brittle or viscous regimes, then the walls will yield and not be able to support large TOP.

(6) In order to explain the non-linear variation of overpressure with channel dip (α) we need to analyse the variations of channel flow patterns with increasing α (Fig. 5). For low α values (15º), the underthrusting motion drags materials to a larger extent into the downward flow, and produces a large vortex in the deeper channel, where the curl dominates the flow field. Consequently, the dynamic pressure remains low. Note that flow divergence increases the dynamic pressure. With increasing α (20º) the flow pattern is characterized by the development of an extrusion channel on the hanging wall side, along which the material extrudes upward with flow convergence at the mouth. Such a negative divergence in the flow builds overpressure on the hanging wall side (Fig. 2D). With further increase in α the extrusion channel widens, and causes the overpressure to drop, as it happens in a pipe flow. This is the reason why the overpressure has a maximum at α around 20-25º.

(7) Inverted metamorphic grade has not been explained by previous models, but the UTC can provide an explanation if one considers the flow pattern shown in Fig. 2B. HP and UHP rocks can be exhumed by two flow cells, both inverting metamorphism because low-grade rocks go down close to the footwall, and high-grade rocks are exhumed close to the hanging wall.

5. Conclusion

The UTC model integrates and provides a robust physical explanation for a number of

561 landmark features in the Greater Himalayan geodynamics, such as simultaneous reverse and
562 normal faulting (channel flow), inversion of the metamorphic grade in the GHS, and exhumation
563 of HP/UHP rocks along a narrow conduit close to the STD. Viscous flow in a UTC involves
564 dynamic pressures in excess of lithostatic pressure, resulting in significant overpressure by a
565 factor more than 1.5, even at depths as shallow as 40 km. The UTC model predicts high pressure
566 (>1.5. GPa) metamorphism of underthrusted rocks, e.g. eclogitization, to occur above 60 km
567 depth. The UTC model shows that the GHS is segmented broadly into two sub-terrains with
568 contrasting pressures: wide southern and narrow northern terranes, with pressures less and
569 greater than 1.5 GPa, respectively. It further shows that temporal variations in channel dip may
570 promote ($\alpha > 15^{o}$) or inhibit ($\alpha < 15^{o}$) exhumation. Overpressure increases with increase in $\boldsymbol{U}$,
571 from $TOP \approx 1.5$ for $\boldsymbol{U}$ = 2-5 cm/yr (current Indian velocity), to $TOP \approx 11$ when $\boldsymbol{U}$ = 20 cm/yr
572 (Indian velocity at 60-70 Ma), which means that in the past all the dynamic processes discussed
573 here may have been enhanced. We tested different model setups (e.g. parallel walls) and
574 boundary conditions (e.g. slip or no-slip condition at bounding walls), but these do not reproduce
575 the prototype. The UTC model shows that tectonic pressure alone can drive the extrusion of HP
576 rocks by channel flow. Viscous deformable walls do not affect overpressure significantly for
577 viscosity contrasts (viscosity walls/viscosity channel) in the order of 1000 or 100. If, during the
578 subduction process, the mouth width, or the dip, or the velocity, or the viscosity, or the
579 conditions at the boundaries change in space and time, then *TOP* will change accordingly, and
580 the exhumation mechanism (flow in the channel) and exhumation depth will also change.
581 *TOP* in a UTC is only possible if the condition at the bottom boundary is not outlet
582 pressure; otherwise it behaves as a leaking boundary that cannot retain dynamic pressure.
583 However, the cold, thick and strong lithospheres that comprise the Indian and Eurasian plates are
584 a good argument against a leaking bottom boundary in a flat-ramp geometry, which means that
585 overpressure can build up to high values in the GHS. The argument does not apply if the channel

586 is “open” at the bottom, because overpressure cannot be retained. This could be the case in
587 subduction zones where there is no evidence for return flow and exhumation concomitant with
588 subduction.

589 The numerical results reported here show that, under specific boundary conditions,
590 geometrical configurations, and parameter sets, high values of overpressure are theoretically
591 possible, which should guide us in the search of new evidence in the natural prototype to prove
592 or disprove the natural existence of high overpressure.

593

594 **Acknowledgements**

595 FOM benefited from a sabbatical fellowship awarded by FCT Portugal
596 (SFRH/BSAB/1405/2014). NM acknowledges DST-SRB, India, for providing a J.C. Bose
597 Fellowship. SG acknowledges funding for doctoral research from the University Grants
598 Commission (UGC/275/Jr Fellow (Sc.)). GR thanks Carleton University for research support.

599

600 **References**

601 Andersen, T.B., Jamtveit, B., Dewey, J.F., Swensson, E., 1991. Subduction and eduction of
602 continental crust: major mechanism during continent–continent collision and orogenic
603 extensional collapse, a model based on the south Caledonides. Terra Nova 3, 303–310.
604 Beaumont, C., Jamieson, R.A., Butler, J.P., Warren, C.J., 2009. Crustal structure: a key constraint
605 on the mechanism of ultra-high-pressure rock exhumation. Earth and Planetary Science Letters
606 287, 116–129.
607 Beaumont, C., Jamieson, R. A., Nguyen, M. H., Lee, B., 2001. Himalayan tectonics explained by
608 extrusion of a low-viscosity crustal channel coupled to focused surface denudation. Nature
609 414, 738–742.
610 Brun, J.-P., Faccenna, C., 2008. Exhumation of high-pressure rocks driven by slab rollback. Earth
611 and Planetary Science Letters 272, 1–7.
612 Burov, E., Jolivet, L., Le Pourhiet, L., Poliakov, A., 2001. A thermomechanical model of
613 exhumation of high pressure (HP) and ultra-high pressure (UHP) metamorphic rocks in
614 Alpine-type collision belts. Tectonophysics 342, 113–136.

615 Burov, E. et al, 2014a. Rheological and geodynamic controls on the mechanisms of subduction
616 and HP/UHP exhumation of crustal rocks during continental collision: Insights from numerical
617 models. Tectonophysics 631, 212-250.
618 Burov, E., François, T., Yamato, P., Wolf, S., 2014b. Mechanisms of continental subduction and
619 exhumation of HP and UHP rocks. Gondwana Research 25, 464–493.
620 Chemenda, A.I., Mattauer, M., Malavieille, J., Bokun, A.N., 1995. A mechanism for syn-
621 collisional rock exhumation and associated faulting: Results from physical modelling. Earth
622 Planet. Sci. Lett. 132, 225–232.
623 Chemenda, A.I., Mattauer, M., Bokun, A.N., 1996. Continental subduction and a mechanism for
624 exhumation of high-pressure metamorphic rocks: new modeling and field data from Oman.
625 Earth and Planetary Science Letters 143, 173–182.
626 Copley, A. & McKenzie, D. 2007.Models of crustal flow in the India-Asia collision zone.
627 Geophysical Journal International, 169, 683–698.
628 Copley, A., Avouac, J. P., Wernicke, B. P., 2011. Evidence for mechanical coupling and strong
629 Indian lower crust beneath southern Tibet. Nature 472, 79–81.
630 Corrie, S.L., Kohn, M.J., Vervoort, J.D., 2010. Young eclogite from the Greater Himalayan
631 Sequence, Arun Valley, eastern Nepal: P–T–t path and tectonic implications. Earth Planet. Sci.
632 Lett. 289, 406–416.
633 DeMets, C., Gordon, R. G., Argus, D. F., 2010. Geologically current plate motions. Geophys. J.
634 Int. 181, 1–80.
635 England, P.C., Holland, T.J.B., 1979. Archimedes and the Tauern eclogites: the role of buoyancy
636 in the preservation of exotic eclogite blocks. Earth and Planetary Science Letters 44, 287–294.
637 England, P. C., Houseman, G. A., 1989. Extension during continental convergence, with
638 application to the Tibetan Plateau. J. Geophys. Res. 94, 17,561 –17,579.
639 Faccenda, M., Minelli, G., Gerya, T.V., 2009. Coupled and decoupled regimes of continental
640 collision: numerical modeling. Earth and Planetary Science Letters 278, 337–349.
641 Feldl, N., Bilham, R., 2006. Great Himalayan earthquakes and the Tibetan plateau. Nature 444,
642 165–170.
643 Ganguly, J., Dasgupta, S., Cheng, W. J., Neogi, S., 2000. Exhumation history of a section of the
644 Sikkim Himalayas, India: records in the metamorphic mineral equilibria and compositional
645 zoning of garnet. Earth Planet. Sci. Lett. 183, 471–486.
646 Gansser, A., 1964. Geology of the Himalayas. Wiley-Interscience, New York, pp. 289.
647 Gerya, T.V., Perchuk, L.L., Burg, J.-P., 2008. Transient hot channels: perpetrating and
648 regurgitating ultrahigh-pressure, high temperature crust–mantle associations in collision belts.

649 Lithos 103, 236–256.
650 Gordon, S.M. et al., 2012. Multi-stage exhumation of young UHP-HP rocks: timescales of melt
651 crystallization in the D'Entrecasteaux Islands, southeastern Papua New Guinea. Earth and
652 Planetary Science Letters 351–352, 237–246.
653 Groppo, C., Lombardo, B., Rolfo, F., Pertusati, P., 2007. Clockwise exhumation path of
654 granulitized eclogites from the Ama Drime range (Eastern Himalayas). J. Metamorph. Geol.
655 25, 51–75.
656 Grujic, D. et al., 1996. Ductile extrusion of the Higher Himalayan Crystalline in Bhutan: evidence
657 from quartz microfabrics. Tectonophysics 260, 21–43.
658 Grujic, D., Warren, C. J., Wooden, J. L., 2011. Rapid synconvergent exhumation of Miocene-aged
659 lower orogenic crust in the eastern Himalaya. Lithosphere 3, 346–366.
660 Hacker, B.R. et al., 2000. Exhumation of ultrahigh-pressure continental crust in east– central
661 China: Late Triassic–Early Jurassic tectonic unroofing. Journal of Geophysical Research 105,
662 13339–13364.
663 Hacker, B.R., Gerya, T.V., 2013. Paradigms, new and old, for ultrahigh-pressure tectonism.
664 Tectonophysics 603, 79-88.
665 Hetényi, G. et al., 2007. Density distribution of the India plate beneath the Tibetan plateau:
666 geophysical and petrological constraints on the kinetics of lower-crustal eclogitization. Earth
667 Planet. Sci. Lett. 264, 226-244.
668 Kellett, D. A., Grujic, D., Coutand, I., Cottle, J., Mukul, M., 2013. The South Tibetan detachment
669 system facilitates ultra rapid cooling of granulite–facies rocks in Sikkim Himalaya. Tectonics
670 32, 252–270.
671 Kylander-Clark, A., Hacker, B., Mattinson, C., 2012. Size and exhumation rate of ultrahigh-
672 pressure terranes linked to orogenic stage. Earth and Planetary Science Letters 321–322, 115–
673 120.
674 Jiménez-Munt,I., Platt,J,P.,2006.Influence of mantle dynamics on the topographic evolution of the
675 Tibetan Plateau: Results from numerical modeling. Tectonics, vol. 25, TC6002,
676 doi:10.1029/2006TC001963
677 Larson, K. P., Ambrose, T. K., Webb, A. G., Cottle, J. M., Shrestha, S., 2015. Reconciling
678 Himalayan midcrustal discontinuities: The Main Central thrust system. Earth Planet. Sci. Lett.
679 429, 139-146.
680 Li, Z., Gerya, T.V., 2009. Polyphase formation and exhumation of high- to ultrahighpressure rocks
681 in continental subduction zone; numerical modeling and application to the Sulu ultrahigh-
682 pressure terrane in eastern China. Journal of Geophysical Research 114 (B9).

683 Little, T.A. et al., 2011. Diapiric exhumation of Earth's youngest (UHP) eclogites in the gneiss
684 domes of the D'Entrecasteaux Islands, Papua New Guinea. Tectonophysics 510, 39–68.
685 Liu, M., Yang, Y., 2003. Extensional collapse of the Tibetan Plateau: results of three-dimensional
686 finite element modeling. Journal of Geophysical Research 108,
687 2361.http://dx.doi.org/10.1029/2002JB002248
688 Malusà, M.G. et al., 2015. Contrasting styles of (U)HP rock exhumation along the Cenozoic Adria-
689 Europe plate boundary (Western Alps, Calabria, Corsica). Geochemistry Geophysics
690 Geosystems 16, 1786-1824.
691 Mancktelow, N., 1995. Nonlithostatic pressure during sediment subduction and the development
692 and exhumation of high pressure metamorphic rocks. J. Geophys. Res. 100, 571–583.
693 Marques, F.O., Ranalli, G., Mandal, N., 2018. Tectonic overpressure at shallow depth in the
694 lithosphere: The effects of boundary conditions. Tectonophysics, in press.
695 Nábělek, J. et al., 2009. Underplating in the Himalaya-Tibet collision zone revealed by the Hi-
696 CLIMB experiment. Science 325, 1371-1374.
697 O'Brien, P. J, Zotov, N, Law, R, Khan, M. A., Jan, M. Q., 2001. Coesite in Himalayan eclogite
698 and implications for models of India-Asia collision. Geology 29, 435–38.
699 Raimbourg, H., Jolivet, L., Leroy, Y., 2007. Consequences of progressive eclogitization on crustal
700 exhumation, a mechanical study. Geophysical Journal International 168, 379–401.
701 Rubatto, D., Chakraborty, S., Dasgupta, S., 2013. Timescales of crustal melting in the Higher
702 Himalayan Crystallines (Sikkim, Eastern Himalaya) inferred from trace element-constrained
703 monazite and zircon chronology. Contrib. Mineral. Petrol. 165, 349–372.
704 Schulte-Pelkum, V. et al., 2005. Imaging the Indian subcontinent beneath the Himalaya.
705 Nature 435, 1222-1225.
706 Sizova, E., Gerya, T.V., Brown, M., 2012. Exhumation mechanisms of melt-bearing ultrahigh
707 pressure crustal rocks during collision of spontaneously moving plates. Journal of
708 Metamorphic Geology 30, 927–955.
709 Sorcar, N., Hoppe, U., Dasgupta, S., Chakraborty, S., 2014. High-temperature cooling histories of
710 migmatites from the High Himalayan Crystallines in Sikkim, India: rapid cooling unrelated to
711 exhumation? Contrib. Mineral. Petrol. 167, 957.
712 Stöckhert, B., Gerya, T.V., 2005. Pre-collisional high pressure metamorphism and nappe tectonics
713 at active continental margins: a numerical simulation. Terra Nova 17, 102–110.
714 Vogt, K., Gerya, T.V., 2014. From oceanic plateaus to allochthonous terranes: numerical
715 modelling. Gondwana Research 25, 494-508.
716 Unsworth, M.J. et al., 2005. Crustal rheology of the Himalaya and Southern Tibet inferred from

717 magnetotelluric data. Nature 438, 78-81.
718 Warren, C.J., 2013. Exhumation of (ultra-)high-pressure terranes: concepts and mechanisms. Solid
719 Earth 4, 75–92.
720 Warren, C.J., Beaumont, C., Jamieson, R.A., 2008. Modelling tectonic styles and ultra-high
721 pressure (UHP) rock exhumation during the transition from oceanic subduction to continental
722 collision. Earth and Planetary Science Letters 267, 129–145.
723 Warren, C.J., Grujic, D., Kellett, D. A., Cottle, J., Jamieson, R. A., Ghalley, K. S., 2011. Probing
724 the depths of the India–Asia collision: U–Th–Pb monazite chronology of granulites from NW
725 Bhutan. Tectonics 30, TC2004.
726 Webb, L.E., Baldwin, S.L., Little, T.A., Fitzgerald, P.G., 2008. Can microplate rotation drive
727 subduction inversion? Geology 36, 823–826.
728 Wobus, C. et al., 2005. Active out-of-sequence thrust faulting in the central Nepalese Himalaya.
729 Nature 434, 1008–1011.
730 Yang, Y., Liu, M., The Indo-Asian continental collision: A 3-D viscous model, Tectonophysics
731 (2013),http://dx.doi.org/10.1016/j.tecto.2013.06.032
732 Zhang, Z. et al., 2015. Oligocene HP metamorphism and anatexis of the Higher Himalayan
733 Crystalline Sequence in Yadong region, east-central Himalaya. Gondwana Research,
734 doi:10.1016/j.gr.2015.03.002.
735 Zhang, Z. et al., 2014. The Moho beneath western Tibet: Shear zones and eclogitization in the
736 lower crust. Earth Planet. Sci. Lett. 408, 370-377.
737
738

Appendix - Methods

Boundary conditions and model setup

The boundary conditions needed to complete the mathematical formulation for numerical simulations were as follows: (1) slab-parallel velocity applied on the underthrusting wall, consistent with the horizontal velocity of the Indian plate (5 cm/yr, DeMets et al., 2010); (2) slip condition on (parallel to) the bottom boundary (Nábělek et al., 2009); (3) no slip condition on the hanging wall; (4) outlet condition with 1 atm pressure at the channel's mouth; (5) gravity applied to the whole channel (~9.8 m/s^2); (6) constant density of the material in the channel = 2800 kg/m^3 (no phase changes in the models), representing the association felsic (mostly) and mafic granulites carrying the eclogite pods. Given that the Indian plate and the TSS above the STD are almost undeformed, attesting to the rigidity contrast between foot and hanging walls of the GHS, the channel walls were assumed undeformable in the simulations, except those testing the effects of viscous walls. In order to investigate flow kinematics and dynamic pressure in the channel, we varied the following parameters: (1) channel viscosity (η), (2) underthrusting velocity ($\boldsymbol{U}$), (3) channel dip (α), (4) channel mouth's width (W_m), and (5) viscosity of channel walls. The viscosity in the channel was varied between 10^{19} and 10^{22} Pa s to cover a broad spectrum of crustal viscosities, as reported in the literature (Beaumont et al., 2001; England and Houseman, 1989; Copley et al., 2011). The current convergence rate between India and Eurasia has been estimated in the order of 5 cm/yr, however, given the wide range of estimated velocities (Feldl and Bilham, 2006; DeMets et al., 2010), we ran numerical simulations varying $\boldsymbol{U}$ between 2 and 20 cm/yr (6.34E-10 to 6.34E-9 m/s in the model). Channel dip was varied between 15 and 30°, which broadly covers the geometry of the GHS shown in different geological sections. We assumed W_m = 25 to 100 km, and W_b (width at the channel's base) = 150 or 200 km, from which we define $W_m^* = W_m/W_b$. We tested a viscosity contrast (viscosity of channel walls/viscosity in the channel) of 1000 to investigate the effects of viscous deformable walls on overpressure.

764 Despite varying all these parameters, the prime focus of our investigation concerned the
765 simulations with $\boldsymbol{U}$ = 5 cm/yr, α = 20°, W_m = 100 km and W_b = 150 km, as they represent the
766 most common and conservative values regarding published data. We then use the numerical
767 results to constrain the viscosity, pressure and velocity in the channel, consistent with current
768 geological data and estimates.

769 The metamorphic processes occur in response to the total isotropic stress, called *dynamic*
770 *pressure*, which is a sum of the tectonic (Stokes) and lithostatic pressures (ρgz, where ρ is
771 density, g is gravitational acceleration, and z is depth) (Figs. A1 and A2). The dynamic pressure
772 results from the viscous flow driven by tectonic stresses in the gravity field. Using the present
773 mechanical model, we evaluate the dynamic pressure to explain the occurrence of high-pressure
774 rocks in the GHS, as a consequence of dynamic pressure in excess of lithostatic pressure at a
775 given crustal depth. We define an overpressure factor (*TOP*) as the non-dimensional ratio
776 between dynamic and lithostatic pressures. For a better understanding of overpressure in a UTC,
777 we carried out a parametric study of *TOP* as a function of η, W_m, α, $\boldsymbol{U}$, and effective
778 convergence velocity (horizontal velocity component > $\boldsymbol{U}$).

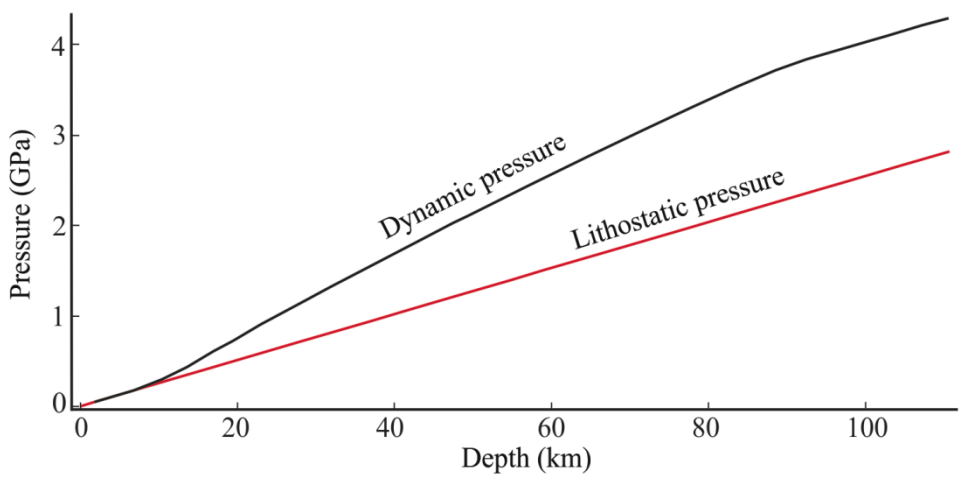

779

780 *Figure A1. Evolution of dynamic and lithostatic pressures in a UTC with* $\eta = 10^{21}$ *Pa s and* ρ =
781 *2800 kg/m*^{3}*. The ratio dynamic pressure/lithostatic pressure corresponds to the overpressure*
782 *factor* (*TOP*).

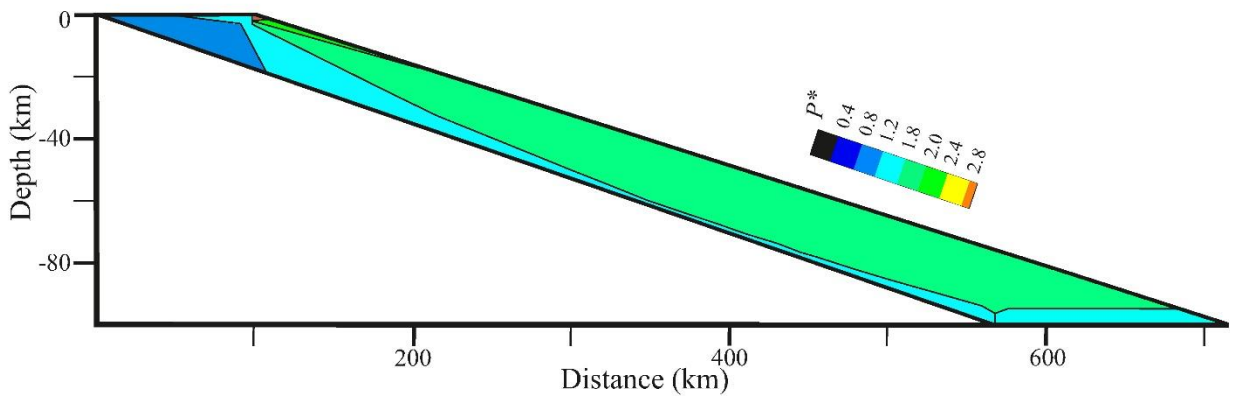

Figure A2. Overpressure in the UTC under the velocity field shown in Fig. 3.

Mathematical formulation

The mathematical model used in the present work is based on the Navier-Stokes equations for two-dimensional steady-state incompressible viscous flows:

$$\rho\left(\frac{\partial \mathbf{u}}{\partial t} + \mathbf{u}\cdot\nabla\mathbf{u}\right) = -\nabla p + \eta\nabla^2\mathbf{u} + \mathbf{F} \quad (1)$$

$$\nabla\cdot\mathbf{u} = 0 \quad (2)$$

where **u** is the velocity vector, p the pressure, ρ the density, η the dynamic viscosity and **F** the external body force (gravity). ρ and η are constant. Then, defining the scaled variables $\bar{x} = x/L$, $\bar{u} = u/U$, $\bar{p} = p/P$ and $\bar{t} = t/T$, in terms of the characteristic length L, velocity U, pressure P and time $T = L/U$, Eqs. (1) and (2) become:

$$\frac{\partial \bar{\mathbf{u}}}{\partial \bar{t}} + \bar{\mathbf{u}}\cdot\bar{\nabla}\bar{\mathbf{u}} = -\mathrm{Eu}\,\bar{\nabla}\bar{p} + \frac{1}{\mathrm{Re}}\bar{\nabla}^2\bar{\mathbf{u}} \quad (3)$$

$$\bar{\nabla}\cdot\bar{\mathbf{u}} = 0 \quad (4)$$

where $\mathrm{Re} = \rho UL/\eta$ and $\mathrm{Eu} = P/\rho U^2$ are, respectively, the Reynolds and Euler numbers. For flows at low characteristic velocity U and high viscosity η, inertial terms Eu and Re in Eq. (3) become negligible. We thus obtain the Stokes approximation of the momentum equation for quasi-static

(creeping) flows, which in dimensional form and under a gravity field reads:

$$-\nabla p + \eta\,\nabla^2 u + \mathbf{F} = 0 \qquad (5)$$

The Stokes equations were solved on the 2-D domain illustrated in Fig. 1C, which was filled with an incompressible viscous linear fluid. The flow equations, with the boundary conditions specified, were solved in the primitive variables $\mathbf{u}\equiv(u,v)$ and p over a finite element mesh, using the algorithm for incompressible Stokes flows implemented in COMSOL.